Article

Next-Generation Multimodality of Nanomedicine Therapy: Folic Acid Conjugated Copolymer and Folate Receptor Interactions Disrupt Receptor Functionality Resulting in Dual Therapeutic Anti-Cancer Potential in Triple-Negative Breast Cancer

Alexandria DeCarlo[1], Cecile Malardier-Jugroot[2,] * and Myron R. Szewczuk[1,]*

[1] Department of Biomedical and Molecular Sciences, Queen's University, Kingston, ON K7L3N6, Canada.
[2] Department of Chemistry and Chemical Engineering, Royal Military College of Canada, Kingston, ON K7K 7B4, Canada
* Correspondence: Tel +1 613 541 6000 ext 6272, Fax +1 613 542 9489. cecile.malardier@mail.mcgill.ca; Tel +1 613 533 2457, Fax +1 613 533 6796.Email: szewczuk@queensu.ca

Abstract: The development of a highly specific drug delivery system (DDS) for anti-cancer therapeutics is an area of intense research focus. Chemical engineering of a "smart" DDS to specifically target tumor cells has gained interest, designed for safer, more efficient, and effective use of chemotherapeutics for the treatment of cancer. However, the selective targeting and choosing the critical cancer surface biomarker are essential for targeted treatments to work. The folic acid receptor alpha (FRα) has gained popularity as a potential target in triple-negative breast cancer (TNBC). We have previously reported on a functionalized folic acid (FA)-conjugated amphiphilic alternating copolymer poly(styrene-*alt*-maleic anhydride) (FA-DABA-SMA) via a biodegradable linker 2,4-diaminobutyric acid (DABA) that has the essential features for efficient "smart" DDS. This biocompatible DDS self-assembles in a pH-dependent manner, providing stimuli-responsive, active targeting, extended-release of hydrophobic chemotherapeutic agents, and can effectively penetrate the inner core of 3-dimensional cancer spheroid models. The empty FA-DABA-SMA decreased spheroid volume, revealing a previously unknown mechanism of action. Upon further investigation, a size- and shape-dependent interaction FA-DABA-SMA with FRα reduced the expression of p53, the product of the highly mutated *TP53* gene, and additional oncogenic c-Myc and STAT3 proteins. Here, we investigated how this copolymer influences FRα behavior and disrupting the receptor's functions. Results indicate that FA-DABA-SMA increases FRα expression levels in breast MDA MB-231 cancer cells and disrupting FRα signaling by the reduction in *HES1* and *NOTCH1* protein expression levels. Also, FA-DABA-SMA induces apoptosis and further causes a change in the morphology of the MDA MB-231 cells, as well as significantly reduces their ability to migrate in a Scratch wound assay. Collectively, these findings provide a novel insight into the functionalized FA-DABA-SMA copolymer. The 350 kDa and 20 kDa copolymers actively target FR*α* to initialize internationalization. However, only the large size and sheet-shaped 350 kDa copolymers disrupt FR*α* signaling. The significance of these novel findings reveals the intracellular activity of the copolymer that is critically dependent on the size and structural shape. This report offers novel therapeutic insight into a dual mechanism of FA-DABA-SMA copolymer for its therapeutic potential for the treatment of cancer.

Keywords: nanoparticles; FA-DABA-SMA; drug delivery systems; folic acid receptor alpha; intracellular disruptions; invasion and migration; breast cancer

 doi:10.20944/preprints202008.0316.v1

1. Introduction

Carcinogenesis is a complex, multifactorial process, and its progression is the result of the manifestation of multiple disease states. The hallmarks of cancer highlight the main components of cancer progression, including sustaining proliferative signaling, evading growth suppressors, activating invasion and metastasis, enabling replicative immortality, inducing angiogenesis, and resisting cell death [1]. Together, these hallmarks only begin to highlight the complexity of the disease, explaining why many treatments are rendered ineffective. As such, the widespread use of cytotoxic chemotherapeutics has reached a therapeutic plateau; however, triple negative breast cancer (TNBC) treatment remains to be mainly limited to chemotherapeutic agents, such as cisplatin, anthracycline, paclitaxel, and tamoxifen (Tmx) [2]. Nevertheless, the efficacy of these treatments is low due to the heterogenic nature of TNBC and the development of resistance. For example, chemotherapy causes the tumor microenvironment (TME) to alter its phenotype in TNBC to become resistant to additional hormonal and chemotherapeutic treatments [2].

Additionally, cancer stem cells (CSCs) are intrinsically resistant to chemotherapy due to their pluripotent and dormant state [3]. CSCs survive through most treatments, mutating to give rise to a more aggressive, resistant phenotype, contributing to metastatic disease, and is prevalent in TNBC [4]. Unfortunately, the treatment of the metastatic disease requires chemotherapeutic agents; thus, we must overcome setbacks, including chemoresistance, poor targeting, poor bioavailability, and high toxicities.

In contrast, targeted therapies are carefully selected therapeutics based on particular molecular alterations driving the transition of more personalized treatment approaches in the era of personalized medicine [5]. Malignant cells often overexpress specific receptors, and sometimes, these become biomarkers for a cancer diagnosis. One such target and biomarkers are gaining popularity it the folate receptor alpha (FRα). Folate is necessary to create a suitable TME as the folate cycle sustains metabolic reactions essential for rapidly growing cells [6]. Folate-mediated one-carbon metabolism (FOCM) is a network of folate-dependent metabolic pathways throughout the cytosol, nucleus, and mitochondria, primarily responsible for DNA and RNA synthesis and methylation of DNA [7]. Cells can direct the flow of one-carbon (1C) units according to cellular demands such as stress conditions, including disease states like cancer [7]. FRα has gained the most attention as it is responsible for the 1C units of folate, essential for the synthesis of DNA and RNA [8]. As such, the application of FRα is extensively studied within the field of oncology as folate dysregulation can result in the disruption of many cell growth-related processes. FRα has been found to overexpressed in a variety of malignancies, including breast, pancreatic, ovarian, colorectal, brain, and lung cancers [9].

FRα is a glycosylphosphatidylinositol (GPI) cell surface protein; however, most normal tissues do not express FRα allowing it to be an accurate target and biomarker of cancer [10]. The low affinity and high capacity reduced folate carrier (RFC) normally mediates folate intake and is distinct from folate receptors, as well as the proton-coupled folate transporter (PCFT) [11]. The main route of transportation of folate is mediated by the RFC, which is responsible for the uptake of dietary folate but is unable to take up anything conjugated with folate [9]. Furthermore, FRα expression in normal tissues is limited to the luminal surface, confined to the apical surface of the epithelium, out of direct contact to any circulating folate or folate receptor targeting agents [10]. When cells become malignant, FRα loses its polarized cellular location, generally restricted to the luminal surface, resulting in the entire surface expressing FRα [10]. Therefore, the low levels of FRα expression in normal tissues, in addition to RFC being unable to take up any conjugated compounds, predicts low toxicity for these targeted agents.

Studies in recent years have begun to focus on FR*α* as a biomarker and target for breast cancer. This approach has become increasingly relevant in treating TNBC as it has limited targetable receptors. FR*α* is overexpressed in breast malignancies with 30% of early-stage breast cancers expressing FR*α* and 70-80% of stage IV metastatic TNBC expressing FR*α* across multiple subtypes [12]. Additionally, FR*α* expression levels are retained in metastatic sites from diverse anatomic origins, including lymph nodes and bones [12]. Therefore, several folate-targeted therapies have

 doi:10.20944/preprints202008.0316.v1

gained popularity. There are multiple ongoing clinical trials for FRα -targeting agents, including several trials specific for TNBC using FRα peptide vaccines and antibody-drug conjugates.

Additional folate-targeting agents include a small molecule drug conjugate and an antibody-drug conjugate, Vintafolide and Farletuzumab, respectively [13,14]. Early-stage clinical data of both of these agents have shown much promise in ovarian and lung cancers with limited toxicity and high response rates [13-16].

Another area of therapeutic advancements is in the development of drug delivery systems (DDSs). DDSs refer to the approaches, technologies, and formulations to achieve the optimized therapeutic effects of drugs in an efficient, specific, and nontoxic manner [17]. DDS nanomaterials provide several benefits due to their unique nanoscale properties, bio-functions, and ability to be easily manipulated, improving previous drug delivery methods [17]. Research into the development of drug delivery vehicles has become increasingly popular in hopes of circumventing limitations associated with traditional drug delivery methods. Nanoparticles (NPs) are defined as particles with a characteristic dimension in the range of 1-100 nm in diameter and are used as potential DDS vehicles [18]. They possess a high drug loading capacity due to their large surface-area-to-volume ratio [19]. NPs can be loaded with a variety of compounds, including small molecules, peptides, proteins, DNA, and interface RNA [20].

NP-based drug delivery offers several advantages compared to free drug treatments, including increased solubility, protection of the loaded drug from degradation or deactivation, increasing bioavailability, controlled release mechanisms, and altered pharmacokinetics [21]. NPs can be engineered with specific properties, including size, shape, and surface modifications to tailor delivery. Finally, NPs can be designed to have an optimal and sustained therapeutic activity through extended-release properties [19].

Multifunctional "smart" NPs are defined as a system with two or more engineered properties [21]. Smart, multifunctional NPs combine targeting strategies to overcome barriers and increase the efficacy of drug delivery. Smart NPs must (i) encapsulate anti-cancer therapeutics, (ii) possess a targeting mechanism to locate malignant tissue effectively, and (iii) respond to stimuli releasing its cargo [18]. Smart NPs ensure that the therapeutic drugs are not released before reaching target tissues, and are only released at a specific rate to provide the most potent and sustained effect [17].

In the present study, we characterized a functionalized NP, as previously reported [22-24]. Here, the functionalized NP is a self-assembled 350 kDa folic acid (FA) conjugated poly(styrene-*alt*-maleic anhydride) (SMA) via biological linker 2,4-diaminobutyric acid (DABA) (FA-DABA-SMA) copolymer. SMA is the polymeric backbone of the NP as it has previously been found to be biocompatible in addition to being capable of being an active drug carrier [22]. At a neutral pH, SMA self-assembles into amphiphilic structures with a 3 nm hydrophobic interior and hydrophilic exterior [22]. This NP property is ideal for chemotherapeutic agents, which are typically hydrophobic and can be encapsulated in the hydrophobic cavity of the NP. Amphiphilic alternating copolymers are advantageous because they can be structurally similar to biological systems as well as have the ability to self-assemble into nanostructures [24]. If the pH increases or decreases, SMA loses its ordered structure, collapsing and releasing its contents progressively in the cellular tumor environment.

Previous studies revealed the empty FA-DABA-SMA copolymer NP reduced breast cancer spheroid volume [23]. This NP was designed to be chemically inert; thus, the mechanism by which the empty FA-DABA-SMA NP reduced spheroid volume was unknown. Further investigations demonstrated a size- and shape-dependent interactions in which the original 350 kDa FA-DABA-SMA continues to induce apoptosis in MDA MB-231 breast cancer cells. In comparison, the 20 kDa FA-DABA-SMA, forming a nanotube structure, did not initiate the same effect [25]. We also found that the interaction of the NP causes intracellular disruptions, reducing the expression of critical proteins, including p53, the product of the highly mutated *TP53* gene, and oncogenic proteins STAT3 and c-Myc [25]. These intracellular disruptions may be due to the interactions of FA-DABA-SMA and FRα possibly dysregulating downstream signaling.

The FRα receptor has become an area of research interest in drug delivery and oncology. The receptor has a high affinity for FA, and cancerous cells overexpress FRα up to two orders in

 doi:10.20944/preprints202008.0316.v1

magnitude relative to non-malignant cells [10,11]. FRα can translocate into the nucleus following FA binding and internalization, suggesting possible activity as a transcription factor for growth-promoting genes, particularly relating to stemness [26]. This observation suggests that FRα may influence the regulation of a variety of malignant processes, including cell growth, cell migration, and epithelial to mesenchymal transition (EMT). The disruption of the regulatory process by FRα may provide a valuable treatment to human cancers. Here, FA-DABA-SMA in our previous studies [24] may be disrupting the interactions of FRα influencing the EMT, an essential component of tumorigenesis and, therefore, warrants further investigations.

The present study characterizes the toxicity, interactions, and secondary intracellular processes of a 350 kDa FA-DABA-SMA copolymer with FAα receptor using prostate and triple-negative breast cancer cell lines. We hypothesize that FA-DABA-SMA interacts with FRα disrupting intracellular processes resulting in a secondary therapeutic mechanism of action, the process of which is size- and shape-dependent dysregulation of FRα.

2. Results

2.1. Folic Acid Supports Cell Growth in Rapidly Proliferating Cells

We have previously reported that the FA-DABA-SMA may have a dual mechanism of action that is size- and shape-dependent [25]. Here, the role of the FA-DABA-SMA may influence cell signaling, possibly contributing to the toxicity seen in the larger sized 350 kDa copolymer. To explore this further, we first asked whether the role of free FA influences cancer cell growth. We have previously demonstrated that the empty FA-DABA-SMA copolymer significantly reduces the cell viability of the MDA MB-231 cell line overexpressing FRα [23,25]. Furthermore, the DU-145 prostate cancer cells were also used because they are metabolically inactive and have been shown to have no significant differences in the cell viability after treatment with FA-DABA-SMA [25].

The benefit of targeting the FRα receptor is that it might confer a growth advantage to the tumor by modulating folate uptake from serum or by generating essential regulatory signals for cell growth [27]. Possibly, FRα may be elevated in some cancers to increase the FA uptake to stimulate the cancer cells to repair DNA damage in transcription factors or other proteins during the early stages of carcinogenesis. Due to the differential carcinogenic roles of FA, it is important to determine if FA has a concentration-dependent effect in DU-145 prostate and MDA MB-231 breast cancer cells. In **Figure 1A,** the data demonstrate a concentration-dependent effect of FA on MDA MB-231 cells, where concentrations higher than 10 μM appear to reduce cell viability. In contrast, there appears to be no difference in cell viability in DU-145 cells (**Figure 1B**) until concentrations reach 40 μM, where there is a reduction in cell viability. These results suggest that the MDA MB-231 cells are more metabolically active over 48 hours and are dependent on FA when compared to DU-145 prostate cancer cells (**Figure 1C and D**). This may, in part, explain the continuous influence FA-DABA-SMA has on MDA MB-231 cells.

Preprints (www.preprints.org) | NOT PEER-REVIEWED | Posted: 14 August 2020 doi:10.20944/preprints202008.0316.v1

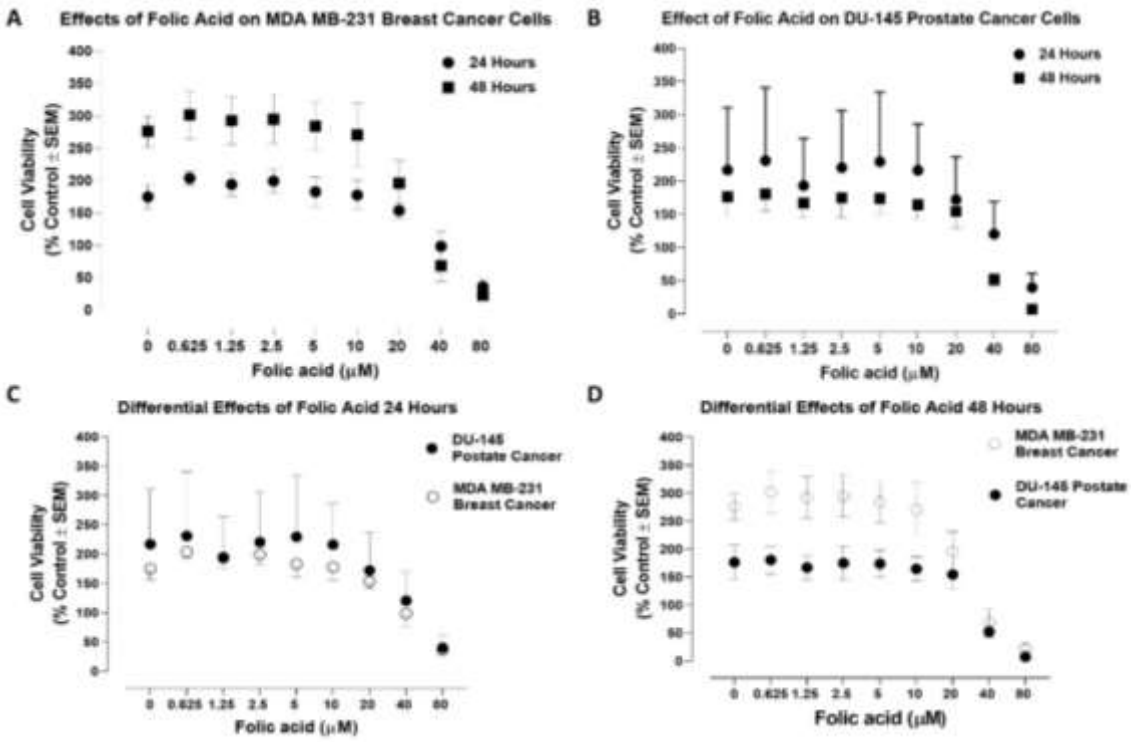

Figure 1. Cell viability of DU-145 and MDA-MB-231 cells following a concentration-dependent treatment with folic acid (FA) using the WST-1 cell proliferation assay. Cells were plated 100 000 cells/mL per well in triplicates. The indicated FA concentrations were serially diluted, and the cells were exposed to the treatments for 24 and 48 hours. At the end of each time point, the WST-1 reagent was added to each well. The cells were incubated for 2 hours, after which the plates were read on a colorimetric plate reader. (A) FA at a concentration of 0.625-10 μM supports MDA-MB-231 breast cancer cell growth over 48 hours. (B) FA does not influence the growth of DU-145 prostate cancer over 48 hours. (C) At 24 hours, the growth of breast and prostate cancer cells is similarly supplemented with FA. (D) At 48 hours, the breast cancer cells increase in cell viability compared to prostate cancer supplemented with FA. The data are presented as cell viability as a mean percent of untreated control ± SEM of two independent experiments (n = 2) performed in triplicates.

2.2. The cytotoxicity of functionalized folic acid-conjugated DABA-SMA is size and shape-dependent

To further explore the possible importance of the functionalized folic acid (FA)-conjugated DABA-SMA copolymer, serial dilutions of the 20 kDa (small), and 350 kDa (large) FA-DABA-SMA were used to compare the cell viability of MDA MB-231 breast and DU-145 prostate cancer cells. Figures 2A and B demonstrate that both the small and large NPs have no effect on DU-145 cell viability at the previously determined 3 μM NP concentration. The 20 kDa small NP did not affect the DU-145 cell viability, even at high concentrations. Similar results are seen with the MDA MB-231 cells (**Figure 2C**). Interestingly, serial dilutions with the 350 kDa larger NP show a decrease in cell viability in DU-145 cells at 6 μM concentrations (**Figure 2B**). These data suggest that the size of the NP is a critical property for the therapeutic potential of FA-DABA-SMA.

Preprints (www.preprints.org) | NOT PEER-REVIEWED | Posted: 14 August 2020 doi:10.20944/preprints202008.0316.v1

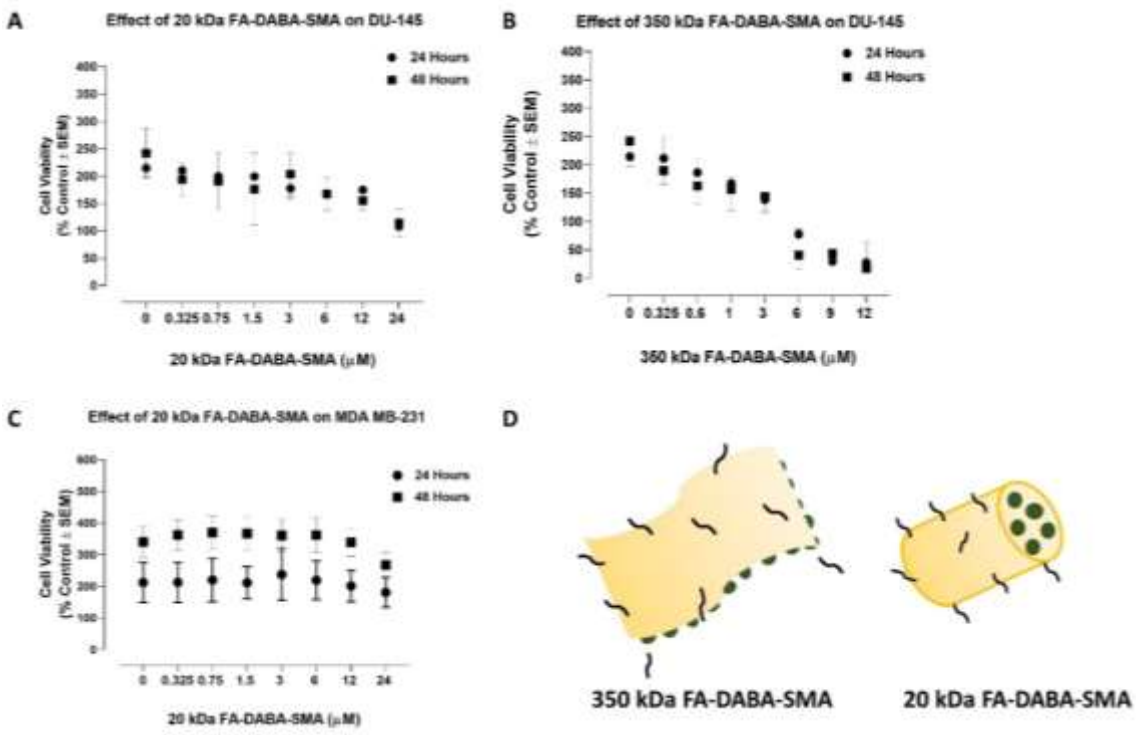

Figure 2. Cell viability of DU-145 and MDA-MB-231 cells following a concentration-dependent treatment with 20 kDa and 350 kDa FA-DABA-SMA copolymer using the WST-1 cell proliferation assay. (A) WST-1 proliferation assay performed in triplicates. The graph represents the mean ± SEM combined results from two independent experiments (n = 2) compared to the untreated control. These results demonstrate that the 20 kDa FA-DABA-SMA does not influence cell viability DU-145 prostate cancer cells over 48 hours of treatment. (B) WST-1 proliferation assay (n = 2) performed in triplicates. The graph represents the mean ± SEM combined results from two independent experiments compared to the untreated control. (C) WST-1 proliferation assay performed in triplicates. The graph represents the mean ± SEM combined results from two independent experiments (n = 2) compared to the untreated control. (D) Schematic of large 350 kDa sheet-shaped FA-DABA-SMA (left) and small 20 kDa cylinder-shaped FA-DABA-SMA.

2.3. Functionalized FA-DABA-SMA induces the Expression of FRα on MDA MB-231 Breast Cancer Cells

We reported that the large 350 kDa FA-DABA-SMA copolymer causes intracellular disruptions of proteins associated with cell growth and proliferation [25]. The mechanism(s) of action for these observations is unknown until now. Here, we hypothesized that the cell surface interactions of the copolymer cause a decrease in cell expression of cell growth and proliferation proteins observed, involving the interaction of the functionalized FA with its FRα target. To investigate this, we first characterized the expression levels of FRα on the cell surface of MDA MB-231 cells. The data depicted in Figure 3A, B, using immunocytochemistry staining with specific anti-FRα antibody confirmed the expression of FRα on MDA-MB-231 cells. To confirm these data, we performed flow cytometry to quantitate the percentage of MDA MB-231 cells expressing FRα (**Figure 3C**).

We also investigated the possible stimulatory effects of the copolymer on FRα following treatment of MDA-MB-231 cells with FA (5 μM), SMA (3 μM), FA-DABA-SMA (3 μM), for 24 and 48 hours. Here, we used the backbone template 350 kDa SMA to confirm that any effects observed at the levels of FRα expression on MDA MB-231 cells were the direct result of the functionalized FA moiety on the copolymer. Interestingly, the treatment with the 350 kDa FA-DABA-SMA over 48 hours significantly increased the percentage of MDA MB-231 cells expressing FRα compared to the untreated controls ($p < 0.01$) and the 350 kDa SMA ($p < 0.05$) as depicted in **Figures 3B and 3C**. These results suggest that the FA-DABA-SMA copolymer has a stimulatory effect of FRα expression on MDA MB-231 cells.

Preprints (www.preprints.org) | NOT PEER-REVIEWED | Posted: 14 August 2020 doi:10.20944/preprints202008.0316.v1

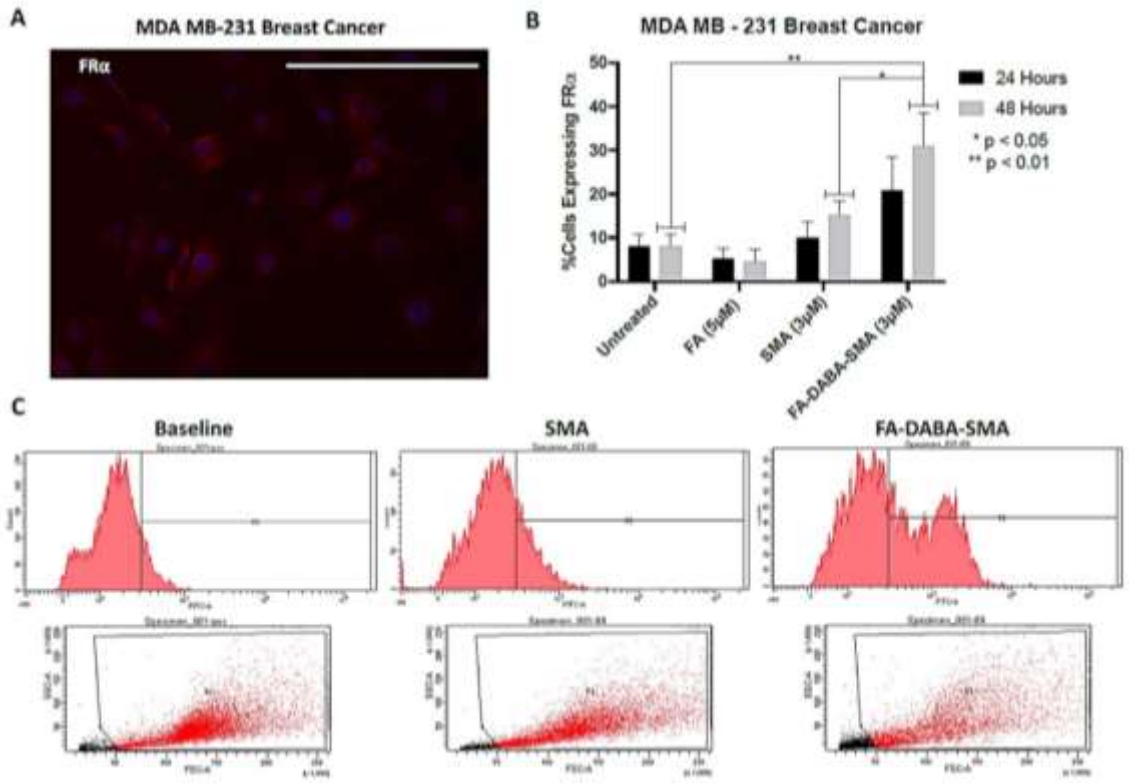

Figure 3. 350 kDa FA-DABA-SMA stimulates FRα expression in MDA MB-231 cells over 48 hours **(A)** Immunocytochemistry staining for FRα in permeabilized MDA-MB-231 cells. Cell images were taken at 400× magnification. Blue DAPI stain represents the nuclei, and red staining is the anti- FRα antibody followed with AlexaFluor 594 secondary antibody for FRα expression. **(B)** Quantification of the percentage of MDA MB 231 cells expressing FRα by flow cytometry at 24 and 48 hours of treatment with FA (3 μM), SMA (3 μM), and FA-DABA-SMA (3 μM) and untreated control. Data represent the mean ± SEM of three independent experiments. The percent cells expressing FRα was compared to the untreated control by ANOVA using the uncorrected Fisher's LSD multiple comparisons test with 95% confidence with indicated asterisks for statistical significance, n = 3. The significance of differences is reported in comparison to the untreated control at the respective time point, and a comparison between SMA and FA-DABA-SMA NPs. (**C)** Representative flow cytometry shifts of 48 hours from one of three experiments showing the increase in FRα expression on the cell surface of MDA-MB-231 cells after treatment with SMA and FA-DABA-SMA and SMA.

It is noteworthy that the functionalized 350 kDa FA-DABA-SMA might have a dual role in increasing FRα expression levels on the cell surface, followed by disrupting the regular FRα functions, as previously observed by the reduction of intracellular proteins. The premise of this concept is that the 350 kDa FA-DABA-SMA induces the expression levels of FRα on MDA MB-231 cells to mediate its dual functionality and cytotoxicity, using its functionalized FA conjugated to the SMA polymer backbone template facilitating active targeting. These findings highlight the importance of receptor biology to gain insight into possible cascade effects and intracellular disruptions occurring in interacting and disrupting normal receptor behavior.

2.4. The Cytotoxicity of FA-DABA-SMA Appears to be Dependent on the Interaction of FA and FRα in MDA MB-231 Breast Cancer Cells

To further assess whether the functionalized 350 kDa FA-DABA-SMA induces apoptosis, MDA MB-231 cells were treated with anti-FRα antibody, FA, FA-DABA-SMA, and SMA at the indicated concentration or left untreated as controls at 24 and 48 hours followed with the CellEvent Caspase 3/7 Green Detection Reagent for 48 hours. As shown in Figure 4, the number of MDA MB-231 cells expressing the caspase 3/7 enzyme increased following treatment with the empty 350 kDa FA-DABA-

Preprints (www.preprints.org) | NOT PEER-REVIEWED | Posted: 14 August 2020 doi:10.20944/preprints202008.0316.v1

SMA at 24- and 48-hour time points. In Figure 4B, caspase levels were analyzed every 2 hours over 48 hours. There is a consistent increase in caspase activity with cells treated with the 350 kDa FA-DABA-SMA (purple) compared to untreated cells (blue) and SMA (red) controls. These results are consistent with the cell viability assay depicted in Figure 4C, where there is a significant ($p < 0.0001$) reduction in cell viability and proliferation in cells treated with the 350 kDa FA-DABA-SMA compared to untreated ($p < 0.0001$) and SMA ($p < 0.0001$) controls.

Interestingly, blocking FRα with anti-FRα antibody or free FA in addition to 350 kDa FA-DABA-SMA, caspase activity decreased as compared to the FA-DABA-SMA treatment alone, as seen in Figure 4B. These data are consistent with the results of the WST-1 proliferation assay depicted in Figure 4C. Additionally, Table 2 highlights the p values of the effect of blocking FRα or adding FA in addition to FA-DABA-SMA. These data, in comparison with the observations with the SMA backbone polymer template having no cytotoxic effect, suggest that the functionalized FA-DABA-SMA copolymer is interacting with FRα and possibly disrupting other signaling pathways involved with apoptosis. These findings support the concept that the functionalized FA on the copolymer is the critical moiety driving the cytotoxicity for 350 kDa FA-DABA-SMA.

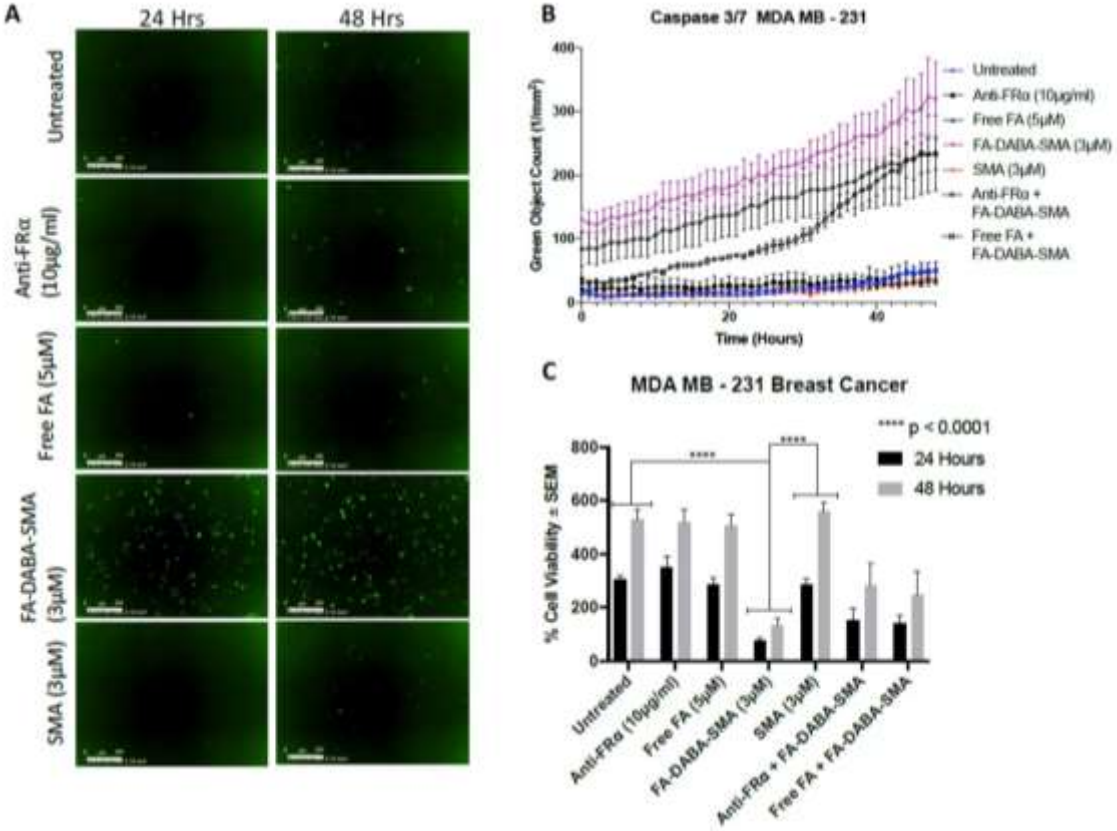

Preprints (www.preprints.org) | NOT PEER-REVIEWED | Posted: 14 August 2020 doi:10.20944/preprints202008.0316.v1

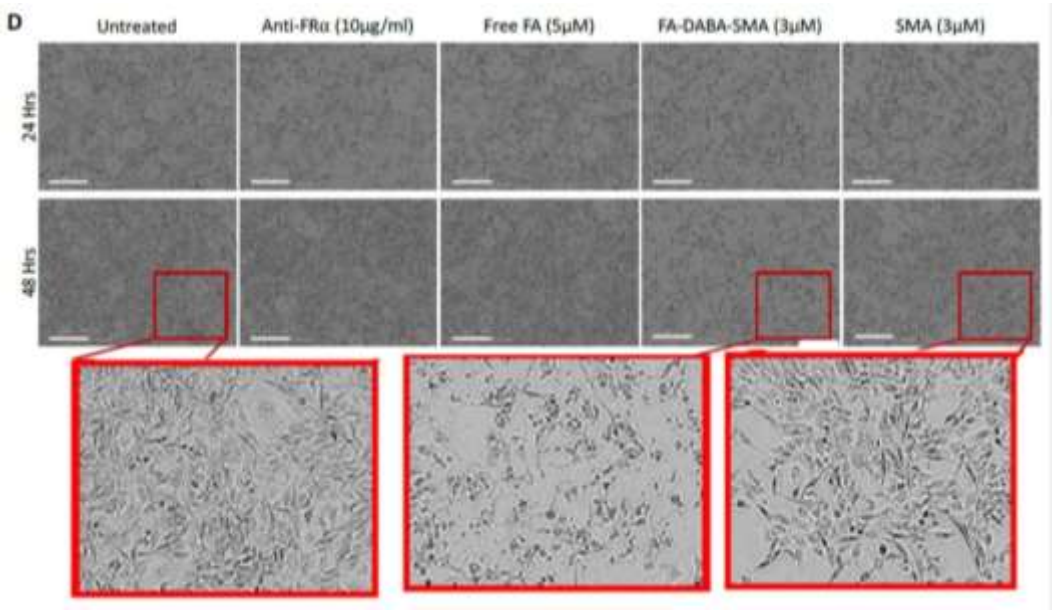

Figure 4. The cytotoxicity of 350 kDa FA-DABA-SMA appears to be due to the interaction of FA and FRα. In contrast, the 350 kDa SMA does not affect caspase activity or cell viability. (A) Cells were plated at 100 000 cells/mL. Cells adhered to the well were treated with the indicated agents followed by CellEvent™ Caspase 3/7 Green Detection reagent added at a concentration of 5 μM in media. Green fluorescent images were acquired by the Incucyte Zoom Imager every 2 hours at 10x magnification. (B) Analyses were done using the Incucyte Zoom Imager Software Analyzer to count the number of expressing Caspase 3/7 (green) cells. The images are representative of two independent experiments performed in triplicates, showing similar results. (C) Comparison of cell viability of MDA MB 231 cells following treatment over 48 hours using the WST-1 assay (n = 3) performed in triplicates. The graph represents the mean ± SEM combined results from two independent experiments compared to the untreated control for each treatment by ANOVA using the uncorrected Fisher's LSD multiple comparisons test with 95% confidence with indicated asterisks for statistical significance. ns, not significant, * $p \leq 0.01$, ** $p \leq 0.001$. (D) FA-DABA-SMA affects the morphology and confluency of MDA MB 231 cells over 48 hours compared to untreated, and SMA treated cells. Pictures representative of three separate experiments (n = 3) performed in triplicates showing similar results. All pictures were taken at 10x magnification and sharpened 100%.

Table 2. Significant *p* values (n = 3, independent experiments) from Figure 4C.

	24 Hours	48 Hours
Untreated vs FA-DABA-SMA	p<0.0001	p<0.0001
Untreated vs anti- FRα + FA-DABA-SMA	p=0.0007	p=0.013
Untreated vs FA + FA-DABA-SMA	p=0.003	p=0.0009
Anti- FRα vs anti- FRα + FA-DABA-SMA	p<0.0001	p=0.004
FA vs FA + FA-DABA-SMA	p=0.001	p=0.0021

In addition to reducing proliferation and inducing apoptosis, the 350 kDa FA-DABA-SMA copolymer causes morphological changes in MDA MB-231 cells at 48 hours of treatment, as depicted in Figure 4D. These morphological cell changes may be due to FA-DABA-SMA disrupting FRα mediated endocytosis. MDA MB-231 cells are typically spindle-shaped and mesenchymal, as seen in the untreated controls and cells treated with the unfunctionalized 350 kDa SMA. This change in the morphological cellular features suggests that there may be a phenotypical transition in these cells, influencing their migratory and invasive potential.

Preprints (www.preprints.org) | NOT PEER-REVIEWED | Posted: 14 August 2020 doi:10.20944/preprints202008.0316.v1

2.5. Functionalized FA-DABA-SMA Reduces the Migratory Potential of MDA MB-231 Breast Cancer Cells in a Scratch Wound Assay

FRα is involved in regulating growth-promoting genes, particularly related to cancer stemness [27]. This concept, together with the morphological changes after treatment with 350 kDa FA-DABA-SMA as seen in Figure 4D, suggests that the effects of the copolymer may also influence the migratory potential of MDA MB-231 cells. Figure 5A depicts the results from a scratch wound assay on untreated controls, 350 kDa SMA, and 350 kDa FA-DABA-SMA on MDA MB-231 cell migration in the scratch wound area over 48 hours. The untreated cells and the unfunctionalized 350 kDa SMA polymer showed near-complete wound closure. In contrast, the 350 kDa FA-DABA-SMA prevented cell migration in the scratch wound closure. Figure 5B represents the quantification of wound width (μm) over 48 hours. Both untreated cells ($p < 0.01$) and those treated with the unfunctionalized 350 kDa SMA ($p < 0.001$) have a significant decrease in wound width (μm) after 48 hours compared to the zero hours, as expected for the migratory potential of MDA MB-232 cells. However, treatment of the cells with the 350 kDa FA-DABA-SMA copolymer drastically disrupts migration in MDA MB-231 cells as there is no significant decrease in wound width (μm) ($p = 0.0589$) over 48 hours. The wound width (μm) remains relatively similar between timepoints. These data suggest that the 350 kDa FA-DABA-SMA copolymer influences migration and invasiveness of MDA MB-231 cells and may alter epithelial-mesenchymal transition (EMT).

To further investigate these phenotypic changes occurring following 350 kDa FA-DABA-SMA treatment of MDA MB-231 cells, HES1 and Notch1 protein levels were examined before and after the treatment of 350 kDa FA-DABA-SMA. FRα binds to its HES1 promoter region. HES1, in particular, is involved in stemness and the generation and regulation of cancer stem cells (CSCs) [28]. Similarly, Notch1 is also related to stemness and influencing EMT [29]. Using Western blot analyses, the data in **Figure 5C** demonstrate the reduction in both HES1 and Notch1 before and after treatment of MDA MB-231 cells with the 350 kDa FA-DABA-SMA copolymer. The quantification of the band densities of the Western blot results presented in **Figure 5D** shows a decrease in protein levels after treatment with 350 kDa FA-DABA-SMA. These results suggest that 350 kDa FA-DABA-SMA copolymer induces a cascade of intracellular disruptions in MDA MB-231 cells, thereby influencing the cell's invasiveness and ability to migrate. This regulatory effect induced by the 350 kDa FA-DABA-SMA copolymer may be due to the disruption of CSCs via the dysregulation of FRα, HES1 and Notch1.

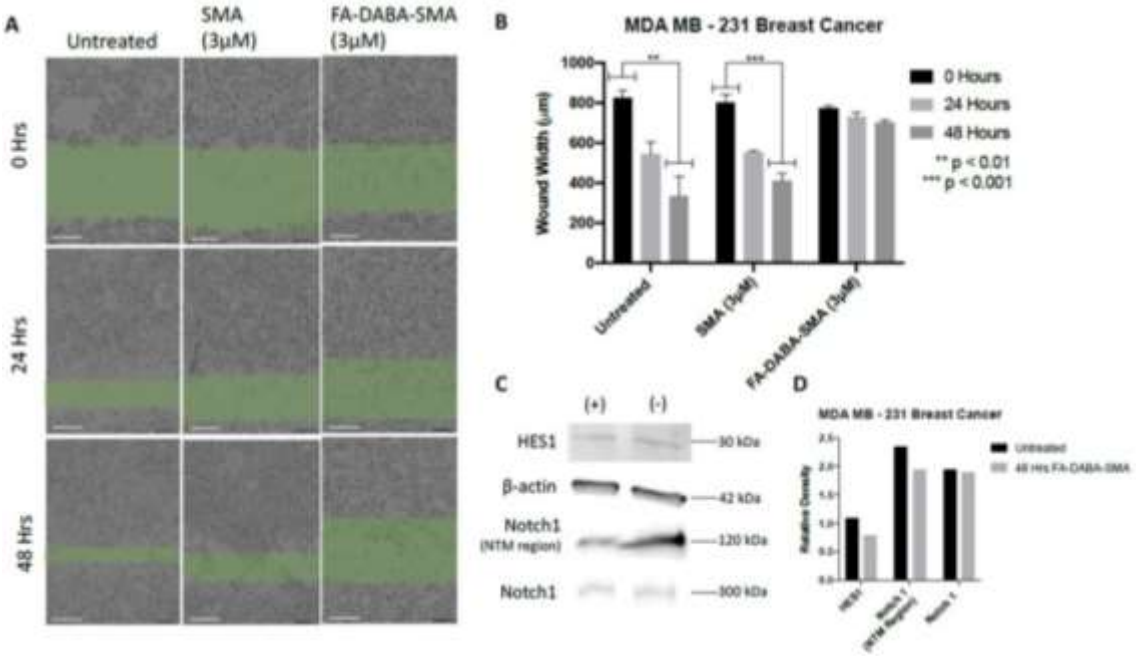

Figure 5. The 350 kDa FA-DABA-SMA blocks the migratory potential of MDA MB-231 cells using the Scratch Wound assay by disrupting Notch1 and HES1 expression. A) FA-DABA-SMA affects the

Preprints (www.preprints.org) | NOT PEER-REVIEWED | Posted: 14 August 2020 doi:10.20944/preprints202008.0316.v1

morphology, confluency, and migration of MDA MB 231 cells over 48 hours compared to untreated, and SMA treated cells using a Scratch Wound assay. Pictures representative of two separate experiments (n = 2) performed in triplicates showing similar results. All pictures were taken at 10x magnification and sharpened 100%. Scale bar represents 300 μm. B) Quantification of wound width (μm) at time 0, 24, and 48 hours. Results were compared by a one-way ANOVA at a 95% confidence using Fisher's LSD test. Error bars represent SEM C) Preliminary western blot analysis showing FA-DABA-SMA decreases HES1 and Notch1 protein levels in MDA MB-231 breast cancer cells after 48 hours (+) compared to untreated controls (-). Data presented as one of two similar experiments (n = 2) D) Quantification of relative band density between untreated and FA-DABA-SMA treated MDA MB 231 breast cancer cells.

2.6. The 350 kDa FA-DABA-SMA Copolymer affects the cell viability of MCF-7 Breast Cancer Cells

Using MCF-7 breast cancer cells, the results in **Figure 6B** indicate that only the functionalized 350 kDa FA-DABA-SMA copolymer reduces the cell viability compared to untreated and SMA controls. These data suggest the implications of NP-cellular interactions through conjugated FA interacting with FRα, and also indicates the possible tissue-specific role of the 350 kDa FA-DABA-SMA is likely due to the differential roles of FA- FRα in different malignancies.

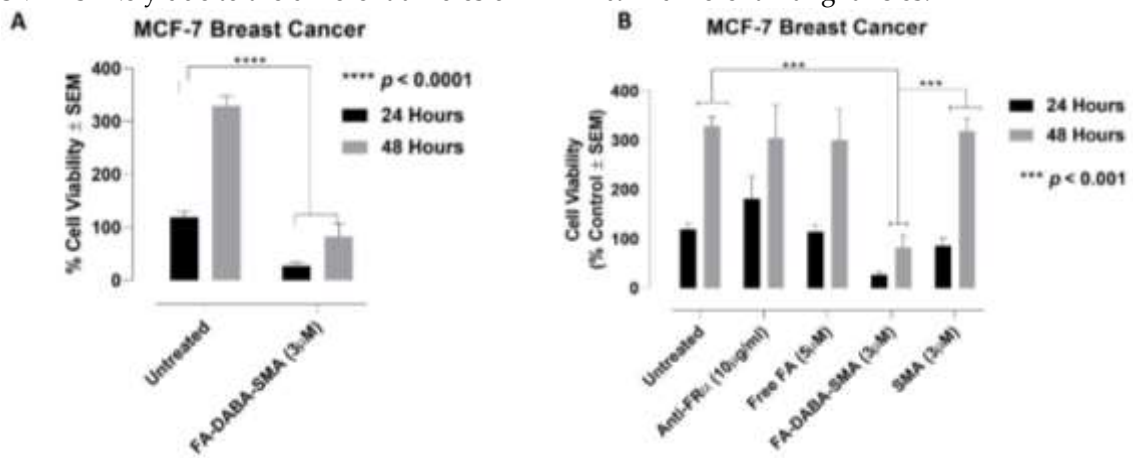

Figure 6. The cell viability of MCF-7 breast cancer cells following treatment with (A) 350 kDa FA-DABA-SMA, and (B) anti-FRα antibody, free FA, and SMA using the WST-1 cell proliferation assay. A) Cells were plated 100 000 cells/mL per well in triplicates. At each time point, the WST-1 reagent was added to each well. The cells were incubated for 2 hours, after which the plates were read on a colorimetric plate reader. The data are cell viability as a mean percent of untreated control ± SEM of three independent experiments performed in triplicates. The cell viabilities were compared to the untreated control for each time point by an unpaired t-test at a 95% confidence. B) WST-1 proliferation assays performed in triplicates. The graph represents the mean ± SEM combined results from three independent experiments compared to the untreated control for each treatment by ANOVA using the uncorrected Fisher's LSD multiple comparisons test with 95% confidence with indicated asterisks for statistical significance. *** $p \leq 0.001$, **** $p \leq 0.0001$.

3. Discussion

Many nanoparticles (NP), mainly with organic properties, are designed to be chemically inert by acting as benign carriers [30]. As our understanding of the physiochemical interactions of NPs within biological systems advances, it is clear that NPs designed to be inert can actively interact with cells, causing a cascade of intracellular disruptions, with the ability to promote therapeutic effects. The nano-biointerface describes the dynamic physiochemical interactions, kinetics, and thermodynamic exchanges between the NP and a biological surface, such as a cell membrane [31]. Understanding these interactions, a point of contact is essential in understanding the functionality and cellular fate of the NP [32].

Typically, active targeting NPs will bind to their target receptor, inducing receptor-mediated endocytosis. The binding of the NP results in a localized decrease in Gibbs free energy allowing the

 doi:10.20944/preprints202008.0316.v1

cell membrane to wrap around the NP, forming a closed vesicle structure [30]. The uptake of NPs is size-dependent, which is likely related to the membrane wrapping process. Since small NPs have less ligand-to-receptor interactions compared to larger NPs, several small NPs need to bind to receptors within proximity in order to produce enough free energy to facilitate membrane wrapping [30]. This concept may explain why the large 350 kDa FA-DABA-SMA continuously influences cell behavior compared to the small-sized 20 kDa FA-DABA-SMA as demonstrated in Figure 2.

The larger NPs also cluster receptors, further promoting cellular uptake [30]. Larger NPs require more receptors facilitating a slower wrapping process. They also tend to arrange themselves linearly, increasing their contact with the cell surface [33]. Internalization is optimized when there is no ligand shortage and no localized receptor shortage on the cell surface [30]. This may explain the stimulatory effect the 350 kDa FA-DABA-SMA to have on FRα expression in MDA MB-23 breast cancer cells (**Figure 3B and C**). It is plausible that the 350 kDa FA-DABA-SMA is clustering FRα requiring more of the receptor to be expressed on the surface instead of intracellularly. This observation may also explain why the non-functionalized 350 kDa SMA backbone template does not have a significant effect on FRα expression levels. The cell-type-specific toxicity of the large 350 kDa FA-DABA-SMA (**Figure 2 and Figure 6**) is dependent on the FRα expression levels, which differ among tissue types, and the differential role of FA in each cell type (**Figure 1**).

The receptor-ligand binding of larger NPs allows for transmembrane penetration due to the interaction force is sufficient. However, this may be harmful to cells as large membrane pores must, therefore, open to allow for particle entry contributing to the toxicity, as seen with the 350 kDa FA-DABA-SMA [34]. Also, simulation studies have now begun to study the NP-cell interface, with a focus on adhesion and possible cytotoxic effects. For example, weak NP-cell adhesion results in insufficient endocytosis, whereas strong NP-membrane adhesion may trap the NP within the membrane, causing a potentially toxic effect and induce apoptosis [35]. Therefore, it is essential to understand the binding activity of the 350 kDa FA-DABA-SMA NP with the cell surface and should be investigated in future studies.

When NPs are internalized via endocytosis, they are then confined to membrane-lined vesicles that are transported throughout the cell. The physiochemical properties of NPs further regulate their interaction with organelles. For example, NP translocation to the nucleus is size-dependent [32]. Additionally, targeting moieties can influence intracellular trafficking, directing NPs to specific organelles [32]. Due to the novel role of FRα translocating to the nucleus and acting as a transcription factor, the functionalized FA-DABA-SMA may facilitate trafficking towards the nucleus causing possible transcriptional disruptions. Such transcriptional disruptions may result in a reduction of protein expression levels, as seen in **Figure 5C and D** and reported in our previous study [25].

The 350 kDa FA-DABA-SMA copolymer is capable of some degree of intracellular trafficking and subsequent cellular disruptions. The active intracellular movement of NPs requires an endosomal escape. pH responsive NPs appear to be particularly ideal [36]. With endosomes and lysosomes having an acidic pH, NPs designed to be reactive to pH collapse from their folded structure, increasing in volume. This increase in volume helps facilitate endosomal escape by causing either an endosome or lysosome to rupture, allowing for the NP to be released within the cytoplasm [36]. Endosomal escape is required to avoid lysosomal degradation of the NP and to facilitate intracellular interactions [36]. Based on the size and pH sensitivity of FA-DABA-SMA, endosomal escape, and intracellular trafficking is apparent and requires further investigation.

The nano-biointerface heavily focuses on the initial point of contact between an NP and the cell surface; however, a sufficient understanding of target receptor biology is crucial in understanding this interface. It is noteworthy that receptors not only provide adhesion force, they also carry translational entropy in which there is redistribution of the receptors on the entire cell membrane [34]. Thus, this nano-biointerface disrupts downstream cell signaling. Additionally, NP-bound ligands can have differential effects on cell signaling when compared with the free ligand [30]. Therefore, the NP surface is a region of highly concentrated ligands, increasing avidity, and potentially altering cell signaling through disrupting regular receptor functions [30].

 doi:10.20944/preprints202008.0316.v1

It is known that FA-FRα signaling is essential during embryogenesis, particularly in neural development, regulating neural crest, and neural tube formation [37,38]. Disruption of this signaling during development results in craniofacial abnormalities, abnormal heart defects, and neural tube defects [38]. Additionally, the role of FRα in maintaining stemness is relatively novel. Specifically, FRα has important transcriptional roles in regulating the expression of pluripotent genes, including *Oct4* and *HES1* [26,37,38]. These genes maintain the stem-like characteristics of neural crest cells while they are migrating during developmental stages [38]. Interestingly, this FA-FRα signaling and regulation of stemness are prevalent in several malignancies [10,39,40]. Therefore, disrupting this signaling may provide significant therapeutic potential.

Results from the present and our other reports demonstrate intracellular disruptions via the interaction with FRα by the decrease in expression of p53, STAT3, c-Myc [25], and HES1 and Notch1 (**Figure 5C and D**) after-treatment of the 350 kDa FA-DABA-SMA. As the 350 kDa FA-DABA-SMA binds to FRα, the receptor function, including localization, may be disrupted. For example, FRα transcriptionally regulates *Oct4*. Interestingly, *Oct4* interacts with STAT3 and c-Myc, where the STAT3/Oct4/c-Myc signaling cascade regulates stemness and mediates doxorubicin resistance in TNBC [41]. The transcriptional role of FRα is disrupted by the 350 kDa FA-DABA-SMA copolymer by dysregulating *Oct4* and subsequently causing a reduction in STAT3 and c-Myc.

Furthermore, the treatment of the 350 kDa FA-DABA-SMA results in morphological changes where the MDA MB-231 cells lose their characteristic spindle-shaped, as demonstrated in **Figure 4D**. This spindle-shape is related to the mesenchymal, stem-like phenotype of aggressive and highly invasive cancer cells, typically mediated by a subpopulation of CSCs [41]. It appears the 350 kDa FA-DABA-SMA reduces the stemness of MDA MB-231 cells as supported by results from **Figure 5,** where there is a reduction in migration and reduced expression of HES1 and Notch1.

CSCs are characterized by their ability to sustain rapid proliferation, self-renewal, invasion, metastasis, and drug resistance [28]. *HES1* is essential in maintaining stem cells in their undifferentiated state [42]. CSCs are similar to normal stem cells in that they maintain an undifferentiated state, are resistant to cell death, and maintain the ability of self-renewal [28]. Specifically, the Notch-HES1 pathway is significant in maintaining breast cancer stem cells, observed in invasive cells, and related to metastasis [28]. Further, during EMT, *HES1* has been found to act as a regulator, inducing, and maintaining phenotypic plasticity [28]. Additionally, genome-wide functional analysis has determined *HES1*, among other novel genes, to regulate p53 activity [43]. *HES1* activates p53 through repressing *HDM2* transcription [43]. Although several mechanisms regulate p53, including localization, phosphorylation, acetylation, and degradation, protein stability is essential. *HDM2* modulates p53 stability, directing nuclear export and proteasomal degradation [43].

HES1 is also regulated by Notch signaling, which can act as an oncogene or tumor suppressor in a cell-type dependent manner [28]. It is, therefore, postulated that cell-type-specific crosstalk occurs between Notch and p53 transduction in which Notch activates p53 by upregulating target genes such as *HES1* [43]. This is further supported by Notch signaling supporting CSC populations in some tumors. For example, when Notch signaling was inhibited in MCF-7 breast cancer cells, there was a significant reduction in tumor-initiating cells, thus eliminating the subpopulation of CSCs [44]. Additionally, the accumulation of the cytoplasmic domain of Notch1 has been reported in many breast cancer cell lines, indicating active Notch signaling supporting CSCs in mammary tissue [44].

In the present study, the 350 kDa FA-DABA-SMA copolymer leads to the reduction of *HES1* and *Notch1*, resulting in morphological changes, reduced migration, and apoptosis. These proteins are a part of the complex, interconnected signaling paradigms regulating stemness, and in some way, are regulated by FRα in breast cancer, as summarized below in Figure 7. This signaling appears to be specific to breast cancer, possibly explaining the cell-type-specific toxicity seen in Figures 2 and 6. In addition to being a drug delivery vehicle, the 350 kDa FA-DABA-SMA copolymer has dual therapeutic anti-cancer potential in disrupting FRα signaling, potentially reducing EMT, stemness, and drug resistance.

Preprints (www.preprints.org) | NOT PEER-REVIEWED | Posted: 14 August 2020 doi:10.20944/preprints202008.0316.v1

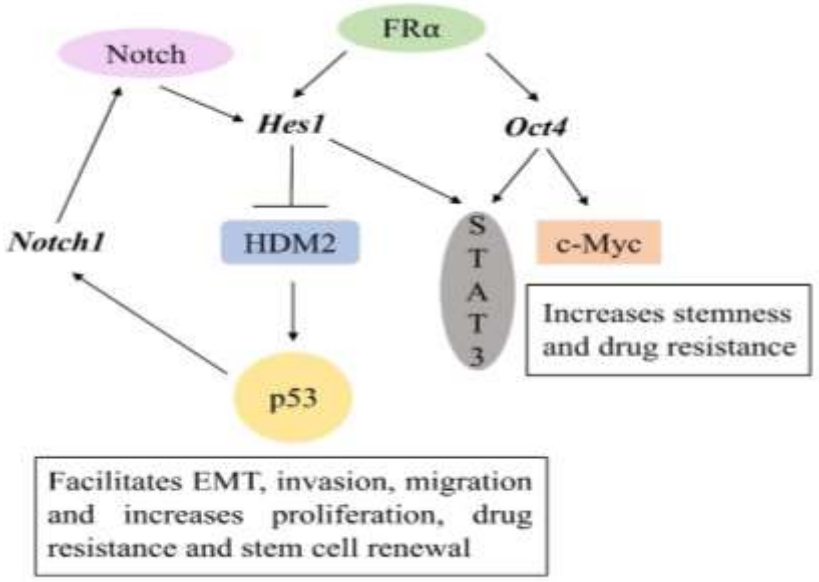

Figure 7. Simplified schematic of possible FRα signaling in breast cancer. FRα transcriptionally regulates *HES1* and *Oct4*. Oct4 interacts with STAT3 and c-Myc to promote stemness and resistance. *HES1* inhibits HDM2 increasing p53 activity. p53 is highly mutated in cancer. Particularly in breast cancer, p53 becomes oncogenic facilitating EMT. Additionally, there is evidence of Notch-HES1 crosstalk further influencing p53 oncogenic activity.

4. Materials and Methods

4.1. Cell Lines and Culturing

MDA MB-231 (ATCC® HTB-26™) is a human triple-negative breast cancer cell line whose site of origin was a metastatic pleural effusion site of a 51-year-old woman with metastatic breast cancer. MDA-MB-231 is a highly aggressive invasive ductal adenocarcinoma and has a genetic profile that expresses *BRAF*, *CDKN2A*, *KRAS*, *NF2*, *TP53*, and *PDGFRA* mutations [45]. MCF-7 (ATCC® HTB-22™) is a human breast adenocarcinoma cell line originating in a metastatic pleural effusion site of a woman 69 years of age with metastatic breast cancer and is ER+. DU-145 (ATCC® HTB-81™) is a human prostate cancer cell line derived from a metastatic brain lesion from a 69-year man with prostate cancer.

All cell lines are grown in standard culture conditions containing 1xDMEM medium supplemented with 10% fetal bovine serum (FBS; HyClone, Logan, UT, USA) and 5µg/mL plasmocin™ (InvivoGen, San Diego, CA, USA). All cells were incubated at 37°C in a 5% CO_2 incubator. Cells were sub-cultured as needed (approximately every 3–5 days) using TrypLE Express (Gibco, Rockville, MD, USA).

4.2. FA-DABA-SMA Copolymer

This copolymer is composed of a hydrophobic group (styrene) alternating with a hydrophilic group (maleic acid) along the polymeric chain (poly (styrene-*alt*-maleic anhydride), SMA). The NP can self-assemble into nanostructures at physiological pH with a hydrophobic inner core allowing for the encapsulation of hydrophobic drugs. Previously, the synthesis of FA-DABA-SMA involves powdered SMA being added to the coupling agent DCC/NHS at a 1:10 ratio with FA-DABA at room temperature and left overnight. FA-DABA-SMA is then dialyzed in water to remove the DMSO solvent and is subsequently freeze-dried. The NP is characterized via HNMR, IR, and DLS. FA-DABA-SMA is dissolved in 10N NaOH and 1 x PBS. 12N HCl is added to bring pH to 7-7.3. Two variations of the NP were used in this study to test the effects of size and shape. The large NP has an

 doi:10.20944/preprints202008.0316.v1

MW of 350,000 g/mol (350kDa) with an Rh of 6 nm and self-assembles into sheets. The small NP has an MW of 20,000 g/mol (20 kDa) with an Rh of 3 nm and self-assembles into cylinders.

4.3. Flow Cytometry

MDA MB-231 cells were harvested and counted for a final concentration of 1.0×10^6 cells/mL. All subsequent steps were done on ice. Cells were washed 2× in 2% FBS + 1× PBS before the primary antibody addition. The cells were treated with 100µL of FRα (MAB5646) primary monoclonal mouse antibody at a final concentration of 10µg/mL and incubated for 60 minutes. Secondary control cells were treated with 100µL of 2% FBS + 1× PBS and incubated for 60 minutes. The cells were then washed 2× with 2% FBS + 1× PBS followed by incubation for 60 minutes with 100µL of secondary anti-mouse antibody AlexaFluor 488 at a final concentration of 10µg/mL. The cells were then washed 2× with 2% FBS + 1× PBS and fixed in 1mL of 4% paraformaldehyde solution before flow cytometry analysis.

4.4. Folic Acid Receptor Alpha

Cells were plated at a density of 10 000 cells/well in 96-well plates for WST-1 experiments, Caspase 3/7 assays, and Live Cell tracking. For Scratch Wound assays, cells were plated at a density of 50 000 cells/well in 96-well plates. Following plating, cells were incubated with 10µg/mL of anti-FRα (MAB5646) antibody for 2 hours to block the FRα. Each experiment type was performed following the respective procedure outlined in each section.

4.5. Immunocytochemistry

Cells were plated at a density of 100 000 cells/mL on glass coverslips in 24 well plates. Cells were treated for 48 hours with empty FA-SMA-DABA. At the end the time point, cells were washed and fixed with 4% PFA for 30 minutes followed by blocking for 1 hour in 10% FBS + 0.1% Triton X-100 + 1x PBS (note: 0.1% Triton x-100 was omitted from blocking buffer for membrane only stains to prevent intracellular non-specific binding). Cells were washed with 1x PBS 3x for 10 minutes followed by the addition of the primary antibody which was diluted to 1:200 or a 10µg/ml concentration using a 1% FBS + 1x PBS + 0.1% Triton X-100 (note: 0.1% Triton x-100 was omitted from antibody buffer for membrane only stains to prevent intracellular non-specific binding) overnight at 4°C. The primary antibody used for these studies was FRα (MAB5646). Cells were washed 3x for 10 minutes with 1x PBS and incubated for 1 hour with AlexaFluor 594 secondary antibodies. Cells were then washed 5x for 10 minutes with 1xPBS (note: one wash included 0.1% Triton x-100 to permeabilize cells for DAPI). DAPI containing mounting media (BioLynx MJS VECTH1200) was added to slides, and coverslips were inverted on to mounting media droplets to counterstain nuclei.

4.6. WST-1 Proliferation Assay

The water-soluble tetrazolium salt-1 (WST-1) assay is a direct measure of metabolically active cells, based on the reduction of a tetrazolium compound to its soluble formazan (orange) derivative by metabolically active cells [46]. The absorbance of the reaction at 420 nm directly correlates to the number of living cells in culture.

Cells were plated at a density of 10 000 cells/well in 96 well plates, incubated, and allowed to adhere overnight. Adhered cells were treated with their respective treatment conditions and concentrations or were left as the untreated controls. At the 24, 48- and 72-hour time points following treatment (Days 1, 2, and 3, respectively), media was removed, and 100µL of 10% WST-1 reagent (Roche Diagnostics, Laval-des-Rapides, QC, Canada) diluted in cell culture media were added to each well. The 96 well plates were then incubated at 37 °C for 2 hours before taking an absorbance reading using the SpectraMax250 machine and SoftMax software. Cell viability measured as a percentage of untreated control was illustrated as a bar graph using GraphPad Prism software (GraphPad Software, La Jolla, CA, USA).

The following formula was used to determine cell viability as a percentage of control (Day 0) after 24, 48, and 72 hours of drug treatment (Days 1, 2 and 3, respectively):

$$\frac{[(absorbance\ in\ given\ drug\ concentration\ on\ day\ 1,\ 2\ or\ 3) - (media\ absorbance)]}{(untreated\ absorbance\ on\ day\ 0) - (media\ absorbance)} \times 100$$

4.7. Caspase 3/7 Assay

Cells were plated at a density of 10 000 cells/well in a 96-well plate and incubated at 37°C in a 5% CO_2 incubator overnight. Cells were treated with 100µL of their respective conditions followed by caspase staining (CellEvent™ Caspase 3/7 Green Detection Reagent, Thermo Fisher Scientific, 168 Third Avenue, Waltham, MA 02451, United States) diluted to the manufacturer's recommended concentration of 5 µM in 5% FBS + 1× PBS from the stock solution of 2 mM. The assay plate was placed in the Incucyte ZOOM® with scan type selected to "caspase 3/7" and running every hour over 48 hrs. Images obtained are representative of 6 images over two separate experiments in triplicates. Image analysis measures fluorescence via Green Object Count per picture ($1/mm^2$).

4.8. Live Cell Imaging

Cells were plated at a density of 10 000 cells/well in a 96-well plate and incubated at 37°C in a 5% CO_2 incubator overnight. 100µL of respective treatments were added to each well. The assay plate was placed in the Incucyte ZOOM® with scans that captured images every 2 hrs over 48 hrs. Phase-contrast images were obtained at 10× magnification and are representative of 6 images over two independent experiments in triplicates.

4.9. Scratch Wound Assay

Cells were plated at a density of 50 000 cells/well in an IncuCyte® ImageLock 96-well plate and incubated at 37°C in a 5% CO_2 incubator for 8-16 hours. Using the WoundMaker™ and following the wounding procedure, precise and reproducible wounds were created in all wells. After wounding, the media were aspirated, and wells were washed up to two times with culture media followed by the addition of 100µL of treatments to each well. The assay plate was placed in the Incucyte ZOOM ® with scan type selected to "scratch wound" and "wide mode" running every 2 hours over 48 hours. Phase-contrast images obtained at 10× magnification and are representative of three separate experiments in triplicates. Wound width was manually measured at three points per image (right, middle, left) to obtain an average. Average wound widths were graphed to show wound closure over 48 hours for each respective well.

4.10. Western Blot

Cells were plated at a density of 600 000 cells/well in a 6-well plate and incubated at 37°C in a 5% CO_2 incubator overnight. Cells were treated with 1mL of their respective treatments. After 48 hours, cells were lysed and centrifuged at 14 000 g for 10 minutes. Protein supernatant was collected, and a DC™ Protein Assay was completed to quantify the amount of protein in the samples. Samples were heated in sample buffer (1:100 ß-mercaptoethanol (BME) to zymogram loading buffer) at 95ºC for 5 minutes. Samples were loaded, and the gel was running at 150V for 90 minutes in a 1x running buffer. Membranes were soaked in methanol for 5 minutes, followed by soaking in blotting buffer for 10 minutes. Sponges and filter paper were soaked in blotting buffer for 10 minutes. Following membrane transfer, the membrane was blocked in 5% skim milk in 1 x TBS for 1 hour at room temperature. The membrane was cut, and primary antibodies were diluted to 1:1000 in 5% skim milk in 1x TBS rocking overnight at 4ºC. Primary antibodies used in this study were HES1 (D6P2U), Notch1 (D1E11), and ß-actin (Sigma A5441). The membrane was washed 3 x 15 minutes in 1x TBS and incubated for 1 hour with secondary antibodies either diluted to 1:3000 for goat-anti mouse IgG HRP (Biorad 170-6516) or 1:10 000 for goat anti-rabbit IgG HRP (Abcam ab97051) in 5% skim milk in 1x TBS. The membrane was washed 3 x 15 minutes in 1 x TBS and then imaged with the Azure c600 Series system. Band densities were quantified using ImageJ.

4.11. Statistical Analysis

Data are presented as the means ± standard error of the mean (SEM) from two or three repeats (n=2 or n=3) of each experiment performed in triplicates. All statistical analyses were performed with GraphPad Prism software. For experiments with three independent experiments, results were either compared with a one-way analysis of variance (ANOVA) at 95% confidence using Fisher's LSD test or results were compared with an unpaired t-test at 95% confidence. Statistical significance is indicated by an asterisk; * $p < 0.05$, ** $p < 0.01$, *** $p < 0.001$ and **** $p < 0.0001$.

5. Conclusions

This report demonstrates the therapeutic potential of a functionalized 350 kDa FA-DABA-SMA copolymer in the treatment of breast cancer. The 350 kDa FA-DABA-SMA is a relevant drug delivery vehicle for breast cancer in addition to being able to disrupt intracellular signaling. There are no implications in targeting FRα as it is not responsible for folate metabolism or cytoplasmic transport of folate. Additionally, healthy breast tissue has highly restricted FRα expression levels, limited to the luminal membrane of secretory ductal cells. Therefore, FRα is a valuable target in several cancers, particularly breast cancer, in which this delivery vehicle therapeutically exploits through dual mechanisms of action.

Author Contributions: Conceptualization, AD, C.M.-J. and MRS; Methodology, AD, C.M.-J. and MRS; Software, AD, and MRS; Validation, AD, C.M.-J. and MRS; Formal Analysis, AD, C.M.-J. and MRS; Investigation, AD, C.M.-J. and MRS; Resources, C.M.-J., MRS; Data Curation, AD, C.M.-J. and MRS; Writing-Original Draft Preparation, A.D., Writing-Review & Editing, AD, C.M.-J. and MRS; Visualization, AD, C.M.-J. and MRS; Supervision, C.M.-J. and MRS; Project Administration, C.M.-J. and MRS; Funding Acquisition, C.M.-J. and MRS.

Funding: This work was supported in part by grants to C Malardier-Jugroot and M R Szewczuk from the Natural Sciences and Engineering Research Council of Canada (NSERC). A. DeCarlo is the recipient of the Queen's University Graduate Award (QGA).

Acknowledgments: We would like to thank Bessi Qorri and Xia Li for their diligent work in fabricating the nanopolymers that were used in this study. Their hard work and attention to detail in the fabrications of the small and large-sized nanopolymers were essential to this study.

Conflicts of Interest: The authors declare no conflict of interest.

References

1. Hanahan, D.; Weinberg, R.A. Hallmarks of cancer: the next generation. *Cell* **2011**, *144*, 646-674, doi:10.1016/j.cell.2011.02.013.
2. Deepak, KGK; Vempati, R.; Nagaraju, GP; Dasari, V.R.; S, N.; Rao, D.N.; Malla, RR Tumor microenvironment: Challenges and opportunities in targeting metastasis of triple negative breast cancer. *Pharmacol Res* **2020**, *153*, 104683, doi:10.1016/j.phrs.2020.104683.
3. Benesch, M.G.K.; Tang, X.; Brindley, D.N. Autotaxin, and Breast Cancer: Towards Overcoming Treatment Barriers and Sequelae. *Cancers (Basel)* **2020**, *12*, doi:10.3390/cancers12020374.
4. Horne, S.D.; Pollick, S.A.; Heng, H.H. Evolutionary mechanism unifies the hallmarks of cancer. *Int J Cancer* **2015**, *136*, 2012-2021, doi:10.1002/ijc.29031.
5. Zugazagoitia, J.; Guedes, C.; Ponce, S.; Ferrer, I.; Molina-Pinelo, S.; Paz-Ares, L. Current Challenges in Cancer Treatment. *Clin Ther* **2016**, *38*, 1551-1566, doi:10.1016/j.clinthera.2016.03.026.
6. Kamen, B.A.; Smith, A.K. A review of folate receptor alpha cycling and 5-methyltetrahydrofolate accumulation with an emphasis on cell models in vitro. *Adv Drug Deliv Rev* **2004**, *56*, 1085-1097, doi:10.1016/j.addr.2004.01.002.
7. Lan, X.; Field, MS; Stover, P.J. Cell cycle regulation of folate-mediated one-carbon metabolism. *Wiley Interdiscip Rev Syst Biol Med* **2018**, *10*, e1426, doi:10.1002/wsbm.1426.
8. Cai, L.; Michelakos, T.; Ferrone, C.R.; Zhang, L.; Deshpande, V.; Shen, Q.; DeLeo, A.; Yamada, T.; Zhang, G.; Ferrone, S., et al. Expression status of folate receptor alpha is a predictor of survival in pancreatic ductal adenocarcinoma. *Oncotarget* **2017**, *8*, 37646-37656, doi:10.18632/oncotarget.16841.

9. Serpe, L.; Gallicchio, M.; Canaparo, R.; Dosio, F. Targeted treatment of folate receptor-positive platinum-resistant ovarian cancer and companion diagnostics, with specific focus on vintafolide and etarfolatide. *Pharmgenomics Pers Med* **2014**, *7*, 31-42, doi:10.2147/PGPM.S58374.
10. Cheung, A.; Bax, H.J.; Josephs, D.H.; Ilieva, K.M.; Pellizzari, G.; Opzoomer, J.; Bloomfield, J.; Fittall, M.; Grigoriadis, A.; Figini, M., et al. Targeting folate receptor alpha for cancer treatment. *Oncotarget* **2016**, *7*, 52553-52574, doi:10.18632/oncotarget.9651.
11. Ledermann, J.A.; Canevari, S.; Thigpen, T. Targeting the folate receptor: diagnostic and therapeutic approaches to personalize cancer treatments. *Ann Oncol* **2015**, *26*, 2034-2043, doi:10.1093/annonc/mdv250.
12. O'Shannessy, D.J.; Somers, E.B.; Maltzman, J.; Smale, R.; Fu, Y.S. Folate receptor alpha (FRA) expression in breast cancer: identification of a new molecular subtype and association with triple negative disease. *Springerplus* **2012**, *1*, 22, doi:10.1186/2193-1801-1-22.
13. Vergote, I.; Leamon, C.P. Vintafolide: a novel targeted therapy for the treatment of folate receptor expressing tumors. *Ther Adv Med Oncol* **2015**, *7*, 206-218, doi:10.1177/1758834015584763.
14. Konner, J.A.; Bell-McGuinn, K.M.; Sabbatini, P.; Hensley, M.L.; Tew, W.P.; Pandit-Taskar, N.; Vander Els, N.; Phillips, M.D.; Schweizer, C.; Weil, S.C., et al. Farletuzumab, a humanized monoclonal antibody against folate receptor alpha, in epithelial ovarian cancer: a phase I study. *Clin Cancer Res* **2010**, *16*, 5288-5295, doi:10.1158/1078-0432.CCR-10-0700.
15. Teng, L.; Xie, J.; Teng, L.; Lee, R.J. Clinical translation of folate receptor-targeted therapeutics. *Expert Opin Drug Deliv* **2012**, *9*, 901-908, doi:10.1517/17425247.2012.694863.
16. Armstrong, D.K.; White, A.J.; Weil, S.C.; Phillips, M.; Coleman, R.L. Farletuzumab (a monoclonal antibody against folate receptor alpha) in relapsed platinum-sensitive ovarian cancer. *Gynecol Oncol* **2013**, *129*, 452-458, doi:10.1016/j.ygyno.2013.03.002.
17. Liu, D.; Yang, F.; Xiong, F.; Gu, N. The Smart Drug Delivery System and Its Clinical Potential. *Theranostics* **2016**, *6*, 1306-1323, doi:10.7150/thno.14858.
18. Hossen, S.; Hossain, M.K.; Basher, M.K.; Mia, M.N.H.; Rahman, M.T.; Uddin, M.J. Smart nanocarrier-based drug delivery systems for cancer therapy and toxicity studies: A review. *J Adv Res* **2019**, *15*, 1-18, doi:10.1016/j.jare.2018.06.005.
19. Kalaydina, R.V.; Bajwa, K.; Qorri, B.; Decarlo, A.; Szewczuk, M.R. Recent advances in "smart" delivery systems for extended drug release in cancer therapy. *Int J Nanomedicine* **2018**, *13*, 4727-4745, doi:10.2147/IJN.S168053.
20. de la Torre, P.; Perez-Lorenzo, M.J.; Alcazar-Garrido, A.; Flores, A.I. Cell-Based Nanoparticles Delivery Systems for Targeted Cancer Therapy: Lessons from Anti-Angiogenesis Treatments. *Molecules* **2020**, *25*, doi:10.3390/molecules25030715.
21. Habibi, N.; Quevedo, D.F.; Gregory, J.V.; Lahann, J. Emerging methods in therapeutics using multifunctional nanoparticles. *Wiley Interdiscip Rev Nanomed Nanobiotechnol* **2020**, 10.1002/wnan.1625, e1625, doi:10.1002/wnan.1625.
22. Li, X.; McTaggart, M.; Malardier-Jugroot, C. Synthesis and characterization of a pH responsive folic acid functionalized polymeric drug delivery system. *Biophys Chem* **2016**, *214-215*, 17-26, doi:10.1016/j.bpc.2016.04.002.
23. Li, X.; Sambi, M.; DeCarlo, A.; Burov, S.V.; Akasov, R.; Markvicheva, E.; Malardier-Jugroot, C.; Szewczuk, M.R. Functionalized Folic Acid-Conjugated Amphiphilic Alternating Copolymer Actively Targets 3D Multicellular Tumour Spheroids and Delivers the Hydrophobic Drug to the Inner Core. *Nanomaterials (Basel)* **2018**, *8*, doi:10.3390/nano8080588.
24. Li, X.; Szewczuk, M.R.; Malardier-Jugroot, C. Folic acid-conjugated amphiphilic alternating copolymer as a new active tumor targeting drug delivery platform. *Drug Des Devel Ther* **2016**, *10*, 4101-4110, doi:10.2147/DDDT.S123386.
25. Sambi, M.; DeCarlo, A.; Malardier-Jugroot, C.; Szewczuk, M.R. Next-Generation Multimodality of Nanomedicine Therapy: Size and Structure Dependence of Folic Acid Conjugated Copolymers Actively Target Cancer Cells in Disabling Cell Division and Inducing apoptosis. *Cancers (Basel)* **2019**, *11*, doi:10.3390/cancers11111698.
26. Boshnjaku, V.; Shim, K.W.; Tsurubuchi, T.; Ichi, S.; Szany, E.V.; Xi, G.; Mania-Farnell, B.; McLone, D.G.; Tomita, T.; Mayanil, C.S. Nuclear localization of folate receptor alpha: a new role as a transcription factor. *Sci Rep* **2012**, *2*, 980, doi:10.1038/srep00980.

27. Kelemen, L.E. The role of folate receptor alpha in cancer development, progression and treatment: cause, consequence or innocent bystander? *Int J Cancer* **2006**, *119*, 243-250, doi:10.1002/ijc.21712.
28. Liu, Z.H.; Dai, X.M.; Du, B. Hes1: a key role in stemness, metastasis and multidrug resistance. *Cancer Biol Ther* **2015**, *16*, 353-359, doi:10.1080/15384047.2015.1016662.
29. Xiao, W.; Gao, Z.; Duan, Y.; Yuan, W.; Ke, Y. Notch signaling plays a crucial role in cancer stem-like cells maintaining stemness and mediating chemotaxis in renal cell carcinoma. *Journal of Experimental & Clinical Cancer Research* **2017**, *36*, 41, doi:10.1186/s13046-017-0507-3.
30. Albanese, A.; Tang, P.S.; Chan, W.C. The effect of nanoparticle size, shape, and surface chemistry on biological systems. *Annu Rev Biomed Eng* **2012**, *14*, 1-16, doi:10.1146/annurev-bioeng-071811-150124.
31. Nel, AE; Madler, L.; Velegol, D.; Xia, T.; Hoek, EM; Somasundaran, P.; Klaessig, F.; Castranova, V.; Thompson, M. Understanding biophysicochemical interactions at the nano-bio interface. *Nat Mater* **2009**, *8*, 543-557, doi:10.1038/nmat2442.
32. Donahue, N.D.; Acar, H.; Wilhelm, S. Concepts of nanoparticle cellular uptake, intracellular trafficking, and kinetics in nanomedicine. *Adv Drug Deliv Rev* **2019**, *143*, 68-96, doi:10.1016/j.addr.2019.04.008.
33. Yue, T.; Zhang, X. Cooperative effect in receptor-mediated endocytosis of multiple nanoparticles. *ACS Nano* **2012**, *6*, 3196-3205, doi:10.1021/nn205125e.
34. Zhang, S.; Gao, H.; Bao, G. Physical Principles of Nanoparticle Cellular Endocytosis. *ACS Nano* **2015**, *9*, 8655-8671, doi:10.1021/acsnano.5b03184.
35. Yue, T.; Zhang, X.; Huang, F. Membrane monolayer protrusion mediates a new nanoparticle wrapping pathway. *Soft Matter* **2014**, *10*, 2024-2034, doi:10.1039/c3sm52659c.
36. Adjei, IM; Sharma, B.; Labhasetwar, V. Nanoparticles: cellular uptake and cytotoxicity. *Adv Exp Med Biol* **2014**, *811*, 73-91, doi:10.1007/978-94-017-8739-0_5.
37. Monick, S.; Mohanty, V.; Khan, M.; Yerneni, G.; Kumar, R.; Cantu, J.; Ichi, S.; Xi, G.; Singh, B.R.; Tomita, T., et al. A Phenotypic Switch of Differentiated Glial Cells to Dedifferentiated Cells Is Regulated by Folate Receptor alpha. *Stem Cells* **2019**, *37*, 1441-1454, doi:10.1002/stem.3067.
38. Mohanty, V.; Shah, A.; Allender, E.; Siddiqui, M.R.; Monick, S.; Ichi, S.; Mania-Farnell, B.; D, GM; Tomita, T.; Mayanil, C.S. Folate Receptor Alpha Upregulates Oct4, Sox2 and Klf4 and Downregulates miR-138 and miR-let-7 in Cranial Neural Crest Cells. *Stem Cells* **2016**, *34*, 2721-2732, doi:10.1002/stem.2421.
39. Scaranti, M.; Cojocaru, E.; Banerjee, S.; Banerji, U. Exploiting the folate receptor alpha in oncology. *Nat Rev Clin Oncol* **2020**, *17*, 349-359, doi:10.1038/s41571-020-0339-5.
40. Holm, J.; Hansen, S.I. Characterization of soluble folate receptors (folate binding proteins) in humans. Biological roles and clinical potentials in infection and malignancy. *Biochim Biophys Acta Proteins Proteom* **2020**, *1868*, 140466, doi:10.1016/j.bbapap.2020.140466.
41. Cheng, C.C.; Shi, L.H.; Wang, X.J.; Wang, S.X.; Wan, X.Q.; Liu, S.R.; Wang, Y.F.; Lu, Z.; Wang, L.H.; Ding, Y. Stat3/Oct-4/c-Myc signal circuit for regulating stemness-mediated doxorubicin resistance of triple-negative breast cancer cells and inhibitory effects of WP1066. *Int J Oncol* **2018**, *53*, 339-348, doi:10.3892/ijo.2018.4399.
42. Goto, N.; Ueo, T.; Fukuda, A.; Kawada, K.; Sakai, Y.; Miyoshi, H.; Taketo, M.M.; Chiba, T.; Seno, H. Distinct Roles of HES1 in Normal Stem Cells and Tumor Stem-like Cells of the Intestine. *Cancer Res* **2017**, *77*, 3442-3454, doi:10.1158/0008-5472.CAN-16-3192.
43. Huang, Q.; Raya, A.; DeJesus, P.; Chao, S.H.; Quon, K.C.; Caldwell, J.S.; Chanda, S.K.; Izpisua-Belmonte, J.C.; Schultz, P.G. Identification of p53 regulators by genome-wide functional analysis. *Proc Natl Acad Sci U S A* **2004**, *101*, 3456-3461, doi:10.1073/pnas.0308562100.
44. Wong, N.K.; Fuller, M.; Sung, S.; Wong, F.; Karsan, A. Heterogeneity of breast cancer stem cells as evidenced with Notch-dependent and Notch-independent populations. *Cancer Med* **2012**, *1*, 105-113, doi:10.1002/cam4.18.
45. Lehmann, B.D.; Bauer, J.A.; Chen, X.; Sanders, M.E.; Chakravarthy, AB; Shyr, Y.; Pietenpol, JA Identification of human triple-negative breast cancer subtypes and preclinical models for selection of targeted therapies. *J Clin Invest* **2011**, *121*, 2750-2767, doi:10.1172/JCI45014.
46. Ngamwongsatit, P.; Banada, P.P.; Panbangred, W.; Bhunia, A.K. WST-1-based cell cytotoxicity assay as a substitute for MTT-based assay for rapid detection of toxigenic Bacillus species using CHO cell line. *J Microbiol Methods* **2008**, *73*, 211-215, doi:10.1016/j.mimet.2008.03.002.